Rheology of 3D Printable Ceramic Suspensions: Effects of Non-Adsorbing Polymer on Discontinuous Shear Thickening

Ria D. Corder,[1,2] **Yuan-Jung Chen,**[1] **Pattiya Pibulchinda,**[1†] **Jeffrey P. Youngblood,**[1] **Arezoo M. Ardekani,**[2] and **Kendra A. Erk**[1*]

[1]School of Materials Engineering, Purdue University, West Lafayette, IN, 47907, USA
[2]School of Mechanical Engineering, Purdue University, West Lafayette, IN, 47907, USA

ABSTRACT

Concentrated suspensions of particles at volume fractions (ϕ) ≥ 0.5 often exhibit complex rheological behavior, transitioning from shear thinning to shear thickening as the shear stress or shear rate is increased. These suspensions can be extruded to form 3D structures, with non-adsorbing polymers often added as rheology modifiers to improve printability. Understanding how non-adsorbing polymers affect the suspension rheology, particularly the onset of shear thickening, is critical to the design of particle inks that will extrude uniformly. In this work, we examine the rheology of concentrated aqueous suspensions of colloidal alumina particles and the effects of adding non-adsorbing polyvinylpyrrolidone (PVP). First, we show that suspensions with ϕ_{alumina} = 0.560-0.575 exhibited discontinuous shear thickening (DST), where the viscosity increased by up to two orders of magnitude above an onset stress (τ_{min}). Increasing ϕ_{alumina} from 0.550 to 0.575 increased the viscosity and yield stress in the shear thinning regime and decreased τ_{min}. Next, PVP was added at concentrations within the dilute and semi-dilute non-entangled regimes of polymer conformation (ϕ_{PVP} = 0.005-0.050) to suspensions with constant ϕ_{alumina} = 0.550. DST was

---

[†] Current address: Northwestern University, Evanston, IL, 60208, USA.
[*] Corresponding author (email: erk@purdue.edu).

observed in all cases and increasing ϕ_{PVP} increased the viscosity and yield stress. Interestingly, increasing ϕ_{PVP} also increased τ_{min}. We posit that the free PVP chains act as lubricants between alumina particles, increasing the stress needed to induce thickening. Finally, we demonstrate through direct comparisons of suspensions with and without PVP how non-adsorbing polymer addition can extend the extrusion processing window due to the increase in τ_{min}.

INTRODUCTION

Particle suspensions at high volume fraction (ϕ) can exhibit complex rheological behavior over a range of increasing shear stresses or shear rates. While dilute suspensions typically exhibit Newtonian flow behavior, shear thickening gradually appears at elevated shear rates for intermediate ϕ ($\approx$ 0.3-0.4).[1,2] This type of shear thickening, in which the viscosity increases by up to several tens of percent, is termed continuous shear thickening (CST).[2] The onset of CST occurs at a critical stress (τ_{min}) which is considered to be roughly independent of ϕ.[2,3] Below τ_{min}, either Newtonian or shear thinning behavior can occur. Upon further increasing ϕ to the concentrated regime ($\geq$ 0.5 for spherical particles), discontinuous shear thickening (DST) often emerges. DST is characterized by a discontinuous jump in viscosity and shear stress above a critical shear rate.[4] The onset of DST occurs at the same τ_{min} as in CST, but DST ends at a maximum stress scale τ_{max} which is also roughly independent of ϕ.[2] Above τ_{max}, shear thinning, strain localization, or bulk/global failure of the suspension can be observed.[5]

Proposed mechanisms underlying DST include hydroclustering,[1] dilatancy,[6] and inter-particle frictional contacts.[7] Traditionally, hydroclustering models were applied to colloidal, Brownian suspensions[3] (particle diameter < 1-2 μm) while dilatancy and frictional models were applied to suspensions of larger, non-Brownian particles[6,8,9] (e.g. aqueous cornstarch suspensions). More recently, the contributions of inter-particle friction to shear thickening of colloidal suspensions have been explored by using simulations and experiments of particles with varying surface roughness[10–13] or adhesion.[12,14] Simulations performed by Mari et al.[15] demonstrate that a geometric framework including a stress-induced friction mechanism unifies the Brownian and non-Brownian regimes, while Jamali and Brady[16] showed that DST arises from restriction in tangential motion which can result from hydrodynamic interactions between rough particles and/or from inter-particle frictional contacts.

Concentrated particle suspensions can be used to fabricate 3D structures through the relatively simplistic technique of direct ink writing (DIW). DIW is a form of filament extrusion 3D printing, where a viscoelastic material is extruded through a nozzle to build up a 3D structure layer-by-layer which then solidifies without the need for additional curing via heat or UV light.[17] This technique is especially suitable for ceramic materials, as ceramic particles can be suspended to facilitate deposition and the printed object is later sintered to form a solid ceramic part.[18–21] Designing suspensions or "inks" for DIW requires a balance to be achieved between material strength and viscosity, as the increasing strength (both elastic modulus and yield stress) that arises from increasing ϕ promotes the formation of self-supporting layers. In contrast, the corresponding increase in viscosity makes the material more difficult to extrude.[17,19] Adsorbing[22] and/or non-adsorbing[20,23] polymers are also often added to DIW inks to improve printability. Since shear thickening is undesirable for extrusion as particle jamming can induce non-uniform flow behavior and eventually clog the deposition nozzle, it is crucial to understand the effects of polymer addition on suspension rheology, particularly on the onset of shear thickening.

The effects of polymers on the shear thickening rheology of particle suspensions have often been explored by means of suspending the particles in polymeric fluids.[24–28] For example, Jain and Shaqfeh[24] reported that suspensions of polyethylene microspheres in a Boger fluid exhibited CST at relatively low ϕ (0.025-0.20) due to particle-induced fluid stresses. Prabhu and Singh[28] dispersed fumed silica nanoparticles in polyethylene glycol carrier fluids of varying molecular weight (MW) and observed that increasing the polymer MW increased suspension viscosity and decreased the onset shear rate of DST. The effects of adsorbing polymers on CST of particles suspended in simple Newtonian fluids have been investigated by Wagner and coworkers,[29–31] demonstrating that adsorbing polymers increase τ_{min} by increasing the hydrodynamic particle diameter and effective particle volume fraction. Bossis et al.[32] examined the effects of adsorbed polymer dispersants on irregularly shaped calcium carbonate particles, observing that addition of a low MW linear polymer led to higher values of τ_{min} of DST compared to addition of larger MW comblike polymers. Park et al.[33] observed that the addition of non-adsorbing polymer depletants at dilute to semi-dilute concentrations enhanced CST and that large MW polymers increased the fraction of particles in contact, promoting the formation of particle contact networks. However, the effects of non-adsorbing polymer addition on DST remain largely unexplored.

In this work, we explore how adding a non-adsorbing polymer, polyvinylpyrrolidone (PVP), affects the rheology of concentrated aqueous suspensions of colloidal alumina particles exhibiting DST. These suspensions also contain a dispersant that coats the surface of alumina particles with anionic moieties. While this system has been 3D printed previously,[20] many other ceramic/dispersant/polymer systems are used in DIW which also exhibit shear thickening.[34–36] First, we present results for alumina particle suspensions with varying $\phi_{alumina}$ within a few percent of the jamming volume fraction and observe how the shear thinning and shear thickening portions of the flow curve are affected by particle loading. Next, we fix $\phi_{alumina}$ and vary ϕ_{PVP} to examine how non-adsorbing polymer addition affects the rheology and, in particular, the onset stress of shear thickening. Finally, we directly compare two sets of suspensions that display similar shear thinning rheology - each set containing one sample with PVP and one without PVP. We conclude with a discussion of the implications of changing the shear thickening onset by PVP addition on material processing for DIW applications.

EXPERIMENTAL SECTION

Materials. Alumina particles (Al_2O_3, batch ground reactive alumina A16 SG, nominal ground median size = 400 nm, Na_2O content = 0.07%, density = 3.95 g/cm^3, Almatis), DARVAN C-N dispersant (ammonium polymethacrylate solution, MW ~ 10000-16000 g/mol, 25% solids, pH 7.5-9.0, density = 1.11 g/cm^3, Vanderbilt Minerals, LLC), and polyvinylpyrrolidone (PVP, MW ~ 55000 g/mol, density = 1.20 g/cm^3, Sigma-Aldrich) were used as received. An SEM image of the ~~bulk~~ colloidal alumina particles, revealing the presence of irregularly shaped particles ~~and aggregates~~, along with the chemical structures of the DARVAN C-N dispersant and PVP, are shown in **Figure 1**.

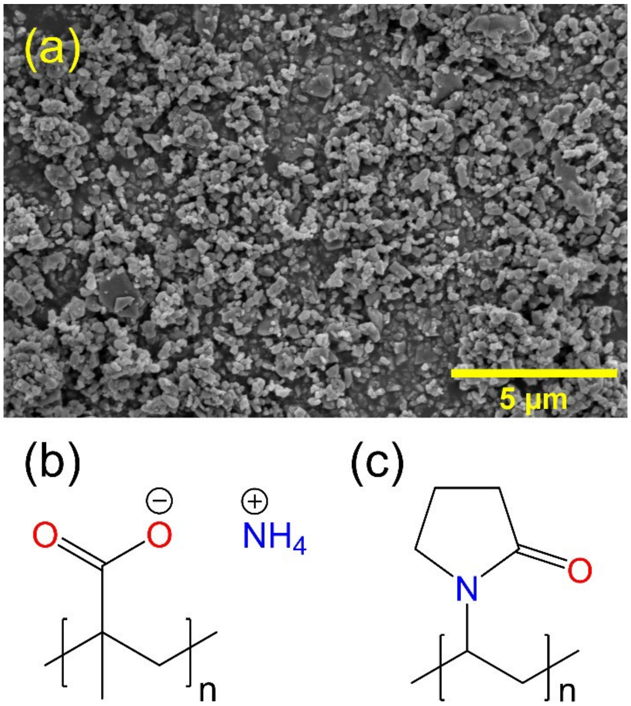

Figure 1. Materials used in this work: (a) SEM image of ~~bulk~~ colloidal alumina particles; chemical structures of (b) DARVAN C-N dispersant (ammonium polymethacrylate), MW = 10000-16000 g/mol and (c) PVP, MW = 55000 g/mol.

Sample preparation. Suspensions without PVP were prepared in 25 mL batches by adding the specified volume fractions by mass of alumina, DARVAN C-N dispersant, and deionized (DI) water to a 125 mL Nalgene® bottle along with zirconia grinding media (10 x 10 mm cylindrical pellets, density = 5.40 g/cm^3, Gilson Company, Inc) equal to 10% of the total suspension volume. Suspensions were mixed via ball milling at 30 rpm for four days with manual stirring via spatula occurring every 24 hours. Ball milling was shown to not affect the alumina particle size but did aid in distribution of the dispersant (**Figure S1** and **Table S1**). For suspensions containing PVP (also prepared in 25 mL batches), the specified volume fraction by mass of PVP and half of the total DI water were added to a 20 mL scintillation vial and dissolved for 24 hours at room temperature under magnetic stirring. The specified volume fractions by mass of alumina and DARVAN C-N dispersant, along with the other half of the DI water and zirconia grinding media equal to 10% of the total suspension volume, were added to a 125 mL Nalgene® bottle and mixed via ball milling at 30 rpm for 24 hours. After 24 hours, the PVP solution was added to the Nalgene® bottle and the suspension was mixed via ball milling at 30 rpm for three more days with manual stirring via spatula occurring every 24 hours. Alumina-free PVP solutions were prepared in 10 mL batches by mixing the specified volume fractions by mass of DARVAN C-N dispersant, PVP, and DI water for 24 hours at room temperature via magnetic stirring.

Particle characterization. ~~The bulk colloidal~~ Alumina particles were pressed into carbon tape and sputter-coated with Au/Pd prior to imaging on a Quanta 650 FEG SEM (FEI) in secondary electron mode with beam voltage = 5 kV and beam current = 0.28 nA. The particle sizes and zeta potentials at 25°C were obtained using a Zetasizer Nano ZS (Malvern Panalytical). Prior to measurement, the suspensions were first diluted by 10^{-6} with DI water and then placed in a bath sonicator for 15 minutes to ensure homogeneous dispersion. The Z-average sizes were measured using disposable plastic cuvettes, while the zeta potentials were measured using a folded capillary zeta cell.

Rheometry. Experiments were performed at 25 °C using an MCR 702 rheometer (Anton Paar) with a CC10 concentric cylinder geometry (bob diameter = 10.0 mm, bob length = 14.9 mm, measuring gap = 0.422 mm). The concentric cylinder geometry was selected to mitigate sample evaporation (which was visually observed to occur within minutes of sample exposure to ambient air) but did not allow for the measurement of normal stresses. Stress-controlled flow sweep experiments were performed on suspensions using a pre-shear conditioning protocol adapted from Lee et al.[31] to break up aggregates and reduce hysteresis. Two cycles of forward and backward stress ramps were performed from 50-500 Pa (30 s/point, 20 points per decade), and then the forward flow sweep data was collected starting from 50 Pa (30 s/point, 20 points per decade) up to the point at which the rheometer's maximum shear rate limit was reached or the sample yielded or fractured. Data from the pre-shear conditioning steps is provided for selected samples in **Figure S2**. Rate-controlled flow sweep experiments were performed on alumina-free PVP solutions using a 30 s pre-shear at 1 s^{-1}, 2 min equilibration, and then a forward shear rate ramp from 1-1000 s^{-1} (30 s/point, 20 points per decade).

Data analysis. All experiments were performed in triplicate and the values reported are averages ± one standard deviation. Experimental data was fitted to theoretical models using Origin 2022 (OriginLab).

RESULTS AND DISCUSSION

Rheology of alumina suspensions. To characterize how the alumina suspensions behave prior to the addition of PVP, a series of suspensions was prepared with increasing ϕ_{alumina} according to the compositions specified in **Table 1**. Addition of a low MW, anionic dispersant forms a thin (< 1 nm) adsorbed layer on the particle surfaces,[23] imparting negative charges which stabilize the alumina suspension via repulsive interactions.[37,38] The ratio of dispersant to alumina was kept constant to maintain a constant particle surface charge across the series of suspensions and was selected based on prior work identifying optimum alumina-PVP suspensions for 3D printing.[20] Representative particle size distributions for each suspension are provided in **Figure S3a**. The particle size and zeta potential data reported in **Table 1** confirm that the size and surface charge remain constant across the series of suspensions.

Table 1. Compositions of suspensions without PVP (vol% alumina, dispersant, PVP, and DI water) and the corresponding Z-average hydrodynamic sizes and zeta potentials.

Alumina (vol%)	**Dispersant (vol%)**	**PVP (vol%)**	**DI water (vol%)**	**Z-average size (nm)**	**Zeta potential (mV)**
55.0	4.20	0	40.8	348 ± 15	-47.9 ± 1.1
55.5	4.24	0	40.3	358 ± 27	-49.2 ± 0.1
56.0	4.28	0	39.7	354 ± 21	-46.0 ± 1.5
56.5	4.32	0	39.2	329 ± 15	-49.9 ± 1.8
57.0	4.35	0	38.6	349 ± 19	-42.6 ± 2.7
57.5	4.39	0	38.1	373 ± 31	-46.6 ± 0.8

Rheological data for these alumina suspensions from the stress-controlled flow sweeps is presented in **Figure 2a** as viscosity vs. shear rate. For all suspensions, shear thinning behavior is observed at low shear rates (viscosity decreases with increasing shear rate). Viscosity increases with increasing $\phi_{alumina}$. Above an onset shear rate, each suspension begins to exhibit shear thickening behavior (viscosity increases with increasing shear rate). This transition occurs at lower shear rates as $\phi_{alumina}$ is increased. For $\phi_{alumina} = 0.550$ and 0.555, the maximum shear rate limit of the rheometer is reached during the shear thickening regime and the experiments were terminated to avoid damaging the instrument. For $\phi_{alumina} \geq 0.560$, the viscosity increases by over two orders of magnitude as the stress ramp progresses. At the start of the shear thickening regime, the shear rate increases with increasing viscosity, then there is a period over which the shear rate decreases with increasing viscosity, up until a point at which the sample yields or fractures and the shear rate increases again. These "S-shaped curves" are characteristic of DST in stress-controlled experiments.[39,40] The scatter in the data in the shear thickening regime suggests the presence of flow inhomogeneities, such as propagating stress fronts[9,41] or density fluctuations.[426]

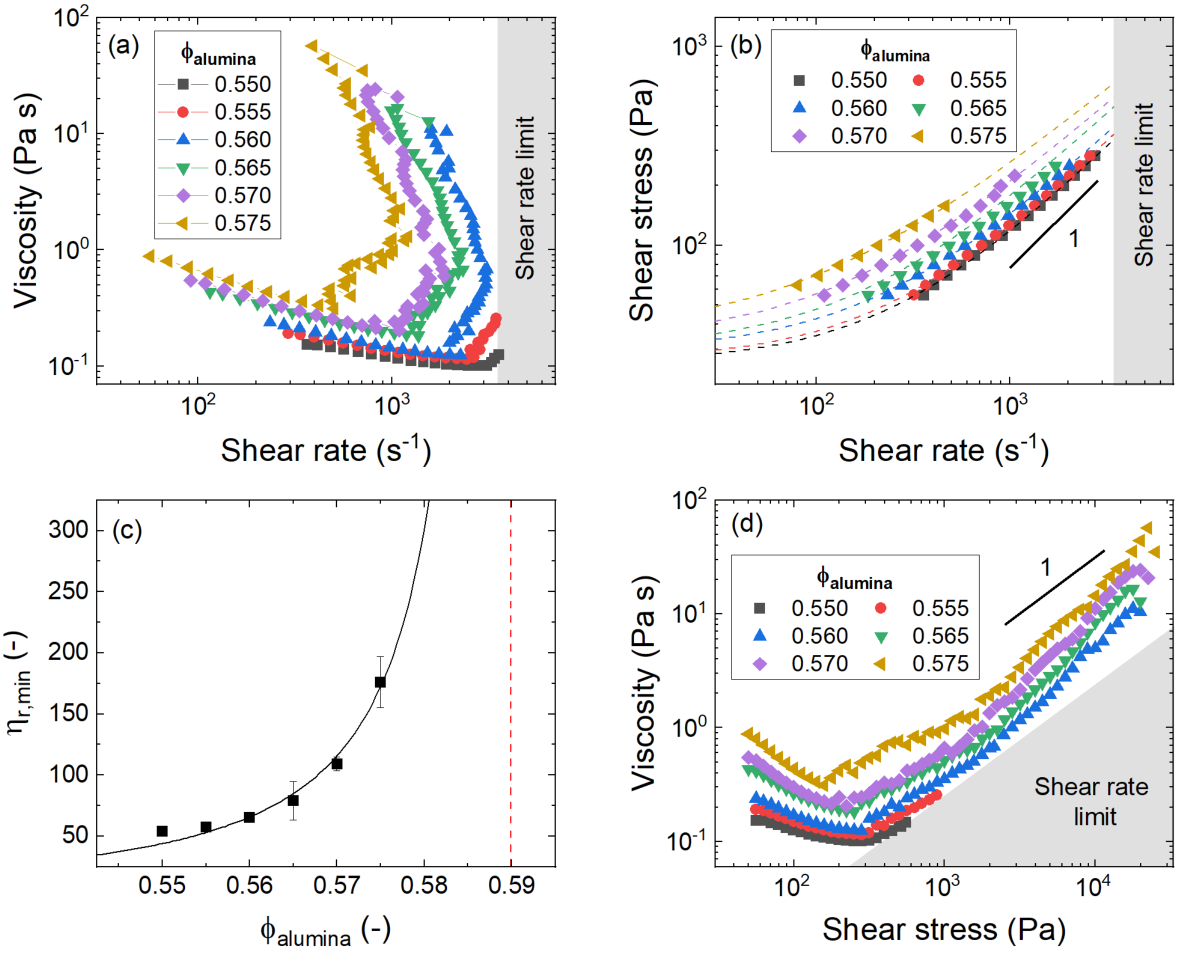

Figure 2. (a) Viscosity vs. shear rate data for alumina suspensions at varying ϕ. The lines between points serve as guides to the eye. (b) Shear stress vs. shear rate data from the shear thinning regime for alumina suspensions at varying ϕ. The dashed lines are the average fits for each ϕ to the Herschel-Bulkley model (Eqn. 1) and the solid black line denotes a slope of 1 indicative of Newtonian flow behavior. (c) Minimum relative viscosity ($\eta_{r,min}$, Eqn. 2) vs. $\phi_{alumina}$. The solid black line is the fit to the generalized Krieger-Dougherty model (Eqn. 3) while the red dashed line denotes the calculated value of the jamming volume fraction, $\phi_j = 0.590$. (d) Viscosity vs. shear stress data for alumina suspensions at varying ϕ. The solid black line denotes a slope of 1 representative of DST. The grey shaded regions in (a), (b), and (d) indicate inaccessible conditions above the maximum shear rate limit.

The data from the shear thinning regimes depicted in **Figure 2a** is next plotted as shear stress vs. shear rate in **Figure 2b**. A slope of 1 on this plot is indicative of Newtonian flow behavior. Each set of shear thinning data can be fitted to the Herschel-Bulkley model, which describes a shear thinning fluid with a dynamic yield stress:[43]

$$\tau = \tau_y + K\dot{\gamma}^n \,, \qquad \text{Eqn. 1}$$

where τ_y is the dynamic yield stress (which dictates the minimum stress required for continuous flow and printing[44]), K is the consistency index, and *n* is the shear thinning index. The dependence of the Herschel-Bulkley fitting parameters on $\phi_{alumina}$ is shown in **Figure 3**. The trends are as expected;[45] with increasing $\phi_{alumina}$, τ_y increases (**Figure 3a**), K increases (**Figure 3b**) and *n* decreases (**Figure 3c**).

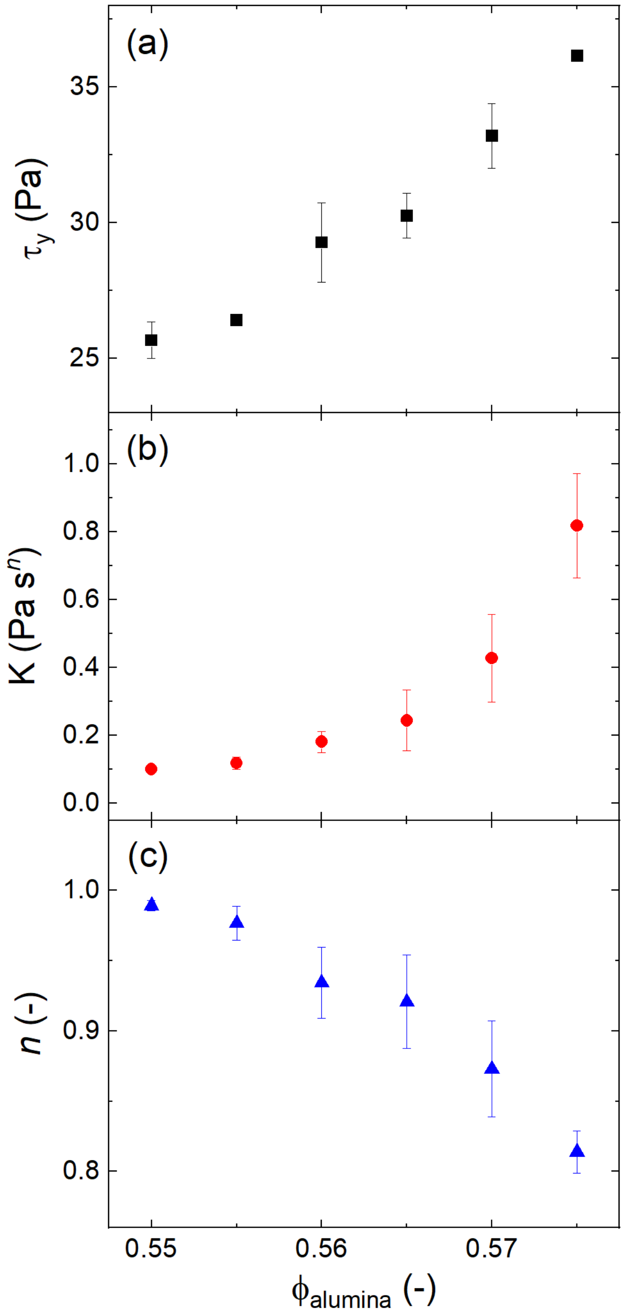

Figure 3. Herschel-Bulkley model (Eqn. 1) fitting results for alumina suspensions at varying ϕ: (a) dynamic yield stress, τ_y; (b) consistency index, K; and (c) shear thinning index, n.

Next, by analyzing how the suspension viscosity depends on $\phi_{alumina}$ the jamming volume fraction (ϕ_J) can be estimated. The following equation is used to calculate the relative minimum viscosity ($\eta_{r,min}$) of each suspension:

$$\eta_{r,min} = \frac{\eta_{min}}{\eta_0} \;, \qquad \text{Eqn. 2}$$

where η_{min} is the lowest viscosity recorded for each suspension (occurring at the onset of shear thickening) and η_0 is the Newtonian viscosity of the suspending medium (measured as ~2 mPa s). The plot of $\eta_{r,min}$ vs. $\phi_{alumina}$ in **Figure 2c** shows that $\eta_{r,min}$ increases exponentially with increasing $\phi_{alumina}$. A generalized Krieger-Dougherty relation[46] can then be used to estimate ϕ_J:

$$\eta_{r,min} = \left(1 - \frac{\phi_{alumina}}{\phi_J}\right)^{-\beta}, \qquad \text{Eqn. 3}$$

where β is a free exponent (usually ≈ 2). Fitting the data in **Figure 2c** to Eqn. 3 results in $\phi_J = 0.590$ ($\beta = 1.41$, $R^2 = 0.938$). This estimation confirms that these suspensions are likely within a few vol% of ϕ_J, where shear thickening can be expected.[2] Further discussion of ϕ_J for these suspensions is presented in the **Electronic Supplementary Information** (**Figure S4**).

The complete flow sweep rheological data from **Figure 2a** is finally plotted as viscosity vs. shear stress in **Figure 2d**. By plotting the data in this manner, the shear stresses at the onset and end of shear thickening (τ_{min} and τ_{max}, respectively) can be readily identified. A slope of 1 on this plot is indicative of DST.[2] **Figure 4** shows the dependence of τ_{min} and τ_{max} on $\phi_{alumina}$. It can be observed from **Figure 4a** that τ_{min} decreases with increasing $\phi_{alumina}$; similar decreases have been observed previously.[5,32,46] This can be attributed to the decreasing inter-particle distance that occurs at higher $\phi_{alumina}$,[47,48] which increases the overall contribution of friction to stress[49] and thus lowers the stress required to overcome the repulsive forces between particles and induce shear thickening. **Figure 4b** shows that τ_{max} increases slightly with increasing $\phi_{alumina}$, a phenomenon which has also been observed previously for suspensions of non-Brownian rod-shaped particles.[50] Gameiro et al.[40] demonstrated that increasing $\phi_{particle}$ increases the persistence of frictional interaction networks (i.e. force chains and loops) during shear thickening. Such an increase in network persistence at increased $\phi_{alumina}$ could allow the suspensions to withstand higher stresses before failure that occurs due to bulk yielding and/or strain localization. In a later section, we explore how these trends with increasing $\phi_{alumina}$ compare to those with increasing non-adsorbing ϕ_{PVP}.

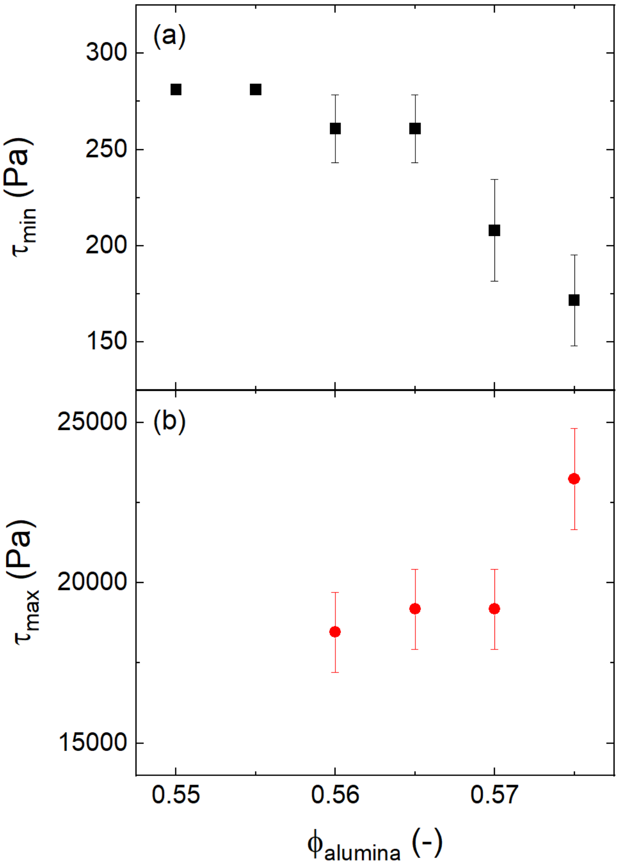

Figure 4. Average stress at (a) onset of thickening (τ_{min}) and (b) end of thickening (τ_{max}) for alumina suspensions at varying ϕ.

Characterization of PVP solution conformation regimes. The interactions between polymer chains in solution are dependent on polymer-solvent affinity and the polymer concentration in the suspending medium.[51] Prior to adding PVP to alumina suspensions, we characterized the polymer conformational dependence on PVP concentration ([PVP]) by preparing a series of solutions containing dispersant, PVP, and DI water (compositions given in **Table S2**). Each of these solutions exhibited Newtonian flow behavior in a shear rate-controlled flow sweep (values provided in **Table S2**). The specific viscosity (η_{sp}) was calculated according to the following equation:

$$\eta_{sp} = \frac{\eta - \eta_0}{\eta_0}, \qquad \text{Eqn. 4}$$

where η is the Newtonian solution viscosity.

The graph of η_{sp} vs. [PVP] in **Figure 5** reveals the presence of three distinct regimes corresponding to different polymer conformations in solution (dilute, semi-dilute non-entangled, and semi-dilute entangled) characterized by different power law scaling exponents. The intersections of the power-law curves identify two critical polymer concentrations: the overlap concentration (c*, the transition between the dilute and semi-dilute non-entangled regimes) and the entanglement concentration (c_e, the transition between the semi-dilute non-entangled and semi-dilute entangled regimes). Using **Figure 5**, we identify c* = 3.93 g/dL and c_e = 20.8 g/dL. Our value of c* for PVP is close to that reported by El Aferni et al.[52] for 55000 g/mol PVP in DI water at 25°C (5.22 g/dL). The slight difference is likely due to the presence of the dispersant occupying some of the solution volumes, causing PVP chains to contact each other at lower concentrations than when the dispersant is absent. Given that much of the dispersant present in the suspension is projected to adsorb onto the alumina particles and not to remain in the suspending medium, we expect that these c* and c_e values are likely lower bounds of where the true transitions occur. Our values for the power law exponents in each of the three regimes are in good agreement with those proposed by Rubinstein and Colby[51] for neutral polymers in good solvents (for the dilute & semi-dilute non-entangled regimes) and athermal solvents (for the semi-dilute entangled regime).

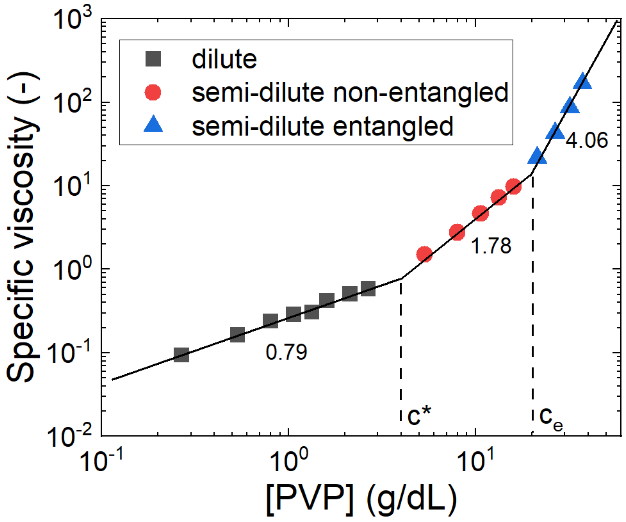

Figure 5. Dependence of specific viscosity (Eqn. 4) on PVP concentration ([PVP]) for alumina-free solutions containing PVP, dispersant, and DI water (compositions specified in Table S2). Three regimes are identified based on the power law scaling exponent corresponding to different polymer conformations in solution: the dilute, semi-dilute non-entangled, and semi-dilute entangled regimes. The intersections of the power law curves identify values for the overlap concentration (c* = 3.93 g/dL) and the entanglement concentration (c_e = 20.8 g/dL).

Effects of PVP addition on alumina suspension rheology. Next, we prepared a series of suspensions with fixed $\phi_{alumina} = 0.550$ and varying ϕ_{PVP} according to the compositions specified in **Table 2**. As before, the ratio of dispersant to alumina was held constant. Representative particle size distributions for each PVP-containing suspension are provided in **Figure S3b**. The particle size and zeta potential data reported in **Table 2** demonstrate that the size and surface charge are unaffected by PVP addition, suggesting that PVP does not interact with the colloidal particle surface and instead locates in the interstitial volume between alumina particles.[23] Using the regimes identified in **Figure 5** and the values for [PVP] given in **Table 2** for $\phi_{alumina} = 0.550$ suspensions with PVP, we estimate that PVP is in the dilute regime for $\phi_{PVP} = 0.005$ and 0.01 and the semi-dilute non-entangled regime for $\phi_{PVP} = 0.03$ and 0.05.

Table 2. Compositions of suspensions containing PVP (vol% alumina, dispersant, PVP, and water), PVP concentration in the suspension ([PVP]), and the corresponding Z-average hydrodynamic sizes and zeta potentials.

Alumina (vol%)	Dispersant (vol%)	PVP (vol%)	DI water (vol%)	[PVP] (g/dL)	Z-average size (nm)	Zeta potential (mV)
55.0	4.20	0.500	40.3	1.33	355 ± 11	-49.4 ± 1.4
55.0	4.20	1.00	39.8	2.66	361 ± 18	-46.6 ± 2.1
55.0	4.20	3.00	37.8	8.00	328 ± 13	-46.6 ± 0.9
55.0	4.20	5.00	35.8	13.3	323 ± 12	-45.3 ± 0.9

Results from stress-controlled flow sweeps on $\phi_{alumina} = 0.550$ suspensions containing varying ϕ_{PVP} are presented in **Figure 6a** as viscosity vs. shear rate. Qualitatively similar behavior is observed here as for the suspensions without PVP (**Figure 2a**); shear thinning behavior at low shear rates, then shear thickening above a critical shear rate, and finally fracturing or yielding after the conclusion of shear thickening. Increasing ϕ_{PVP} increases the suspension viscosity in the shear thinning regime and decreases the critical shear rate at which the transition from shear thinning to shear thickening occurs. "S-shaped" curves are again observed in the shear thickening regime. Scatter in the data is reduced in the latter part of the shear thickening regime (where shear rate decreases as the viscosity increases) for $\phi_{PVP} \geq 0.01$ compared to the PVP-free suspensions in **Figure 2a**, suggesting that the presence of PVP may suppress flow inhomogeneities.

The shear thinning data for each suspension containing PVP is plotted in **Figure 6b** as shear stress vs. shear rate. The trends in the Herschel-Bulkley fitting parameters (Eqn. 2) with varying ϕ_{PVP} (**Figure 7**) follow similar trends to those observed in **Figure 3**: with increasing ϕ_{PVP}, we observe increasing τ_y (**Figure 7a**), increasing K (**Figure 7b**) and decreasing n (**Figure 7c**). Notably, higher values of τ_y are achieved by PVP addition (**Figure 7a**) than by alumina addition (**Figure 3a**) This can be attributed to strong attractions formed by nonequilibrium osmotic forces present during exclusion of depletant molecules from inter-particle gaps.[33,53] Higher τ_y and lower n values are desirable for DIW applications to maintain layer integrity of printed parts while allowing extrusion of the suspension through fine nozzles.[19,54]

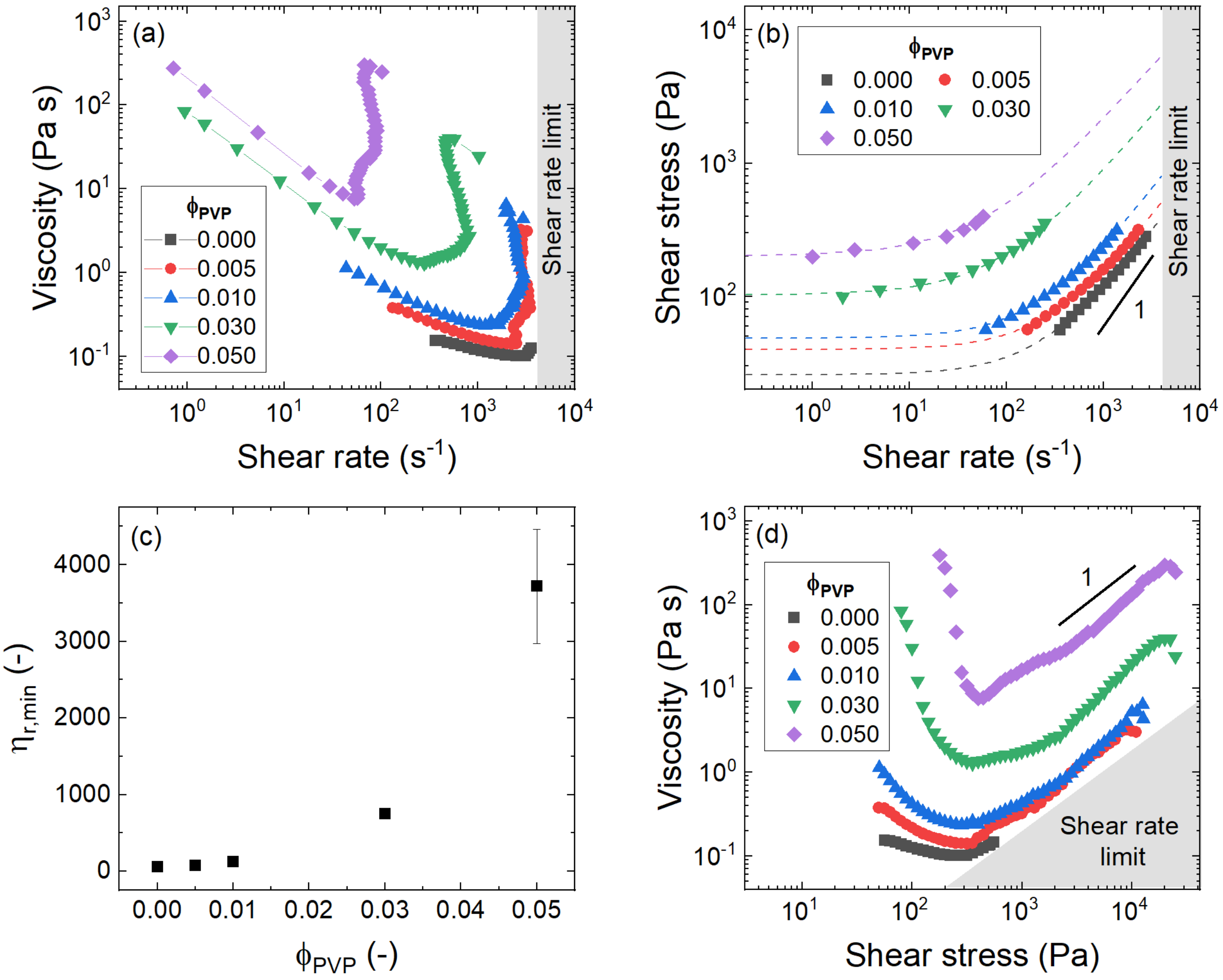

Figure 6. (a) Viscosity vs. shear rate data for $\phi_{alumina} = 0.550$ suspensions at varying ϕ_{PVP}. Lines between points serve as guides to the eye. (b) Shear stress vs. shear rate data from the shear thinning regime for $\phi_{alumina} = 0.550$ suspensions at varying ϕ_{PVP}. The dashed lines are the average fits for each ϕ to the Herschel-Bulkley model (eqn. 1), and the solid black line denotes a slope of 1 indicative of Newtonian flow behavior. (c) Minimum relative viscosity ($\eta_{r,min}$, eqn. 2) vs. ϕ_{PVP}. (d) Viscosity vs. shear stress data for $\phi_{alumina} = 0.550$ suspensions at varying ϕ_{PVP}. The solid black line denotes a slope of 1 representative of DST. The grey shaded regions in (a), (b), and (d) indicate inaccessible conditions above the maximum shear rate limit.

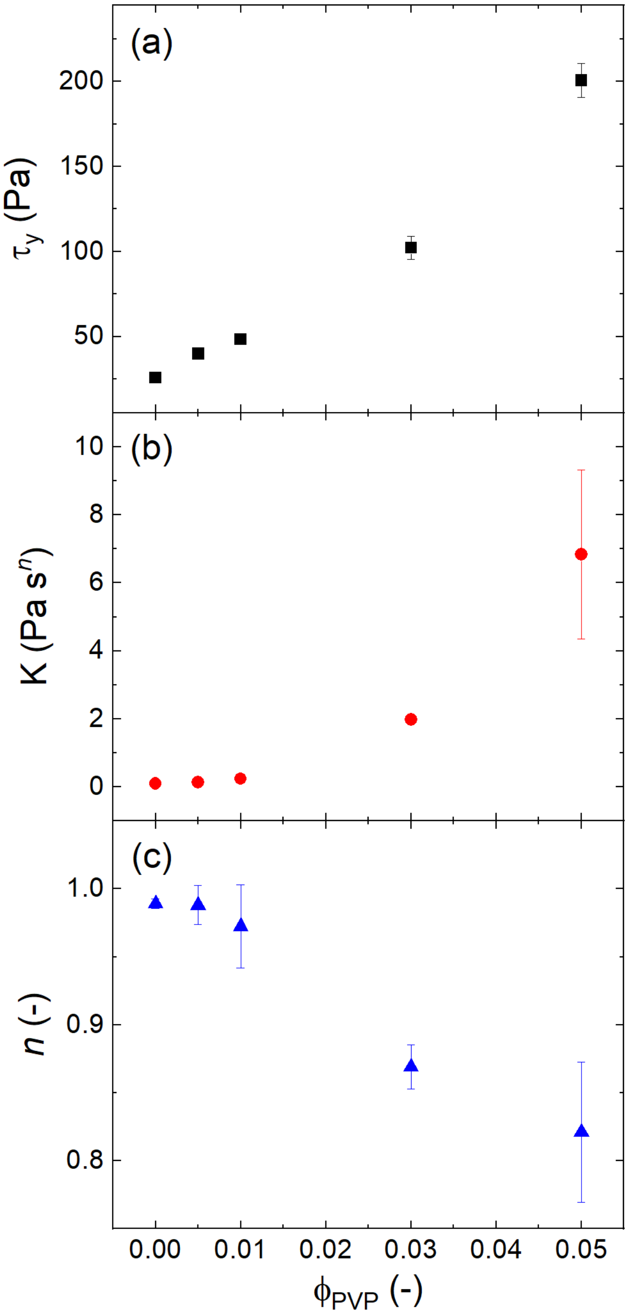

Figure 7. Herschel-Bulkley model (Eqn. 1) fitting results for $\phi_{alumina} = 0.550$ suspensions at varying ϕ_{PVP}: (a) dynamic yield stress, τ_y; (b) consistency index, K; and (c) shear thinning index, n.

In **Figure 6c**, it is shown that $\eta_{r,min}$ (Eqn. 2) exponentially increases with ϕ_{PVP} in a similar manner as in **Figure 2c**. Notably, the highest $\eta_{r,min}$ achieved for $\phi_{PVP} = 0.050$ is an order-of-magnitude higher than that recorded for $\phi_{alumina} = 0.575$, again highlighting the strong effects of non-adsorbing polymer addition on the concentrated suspension rheology.

Lastly, the data for PVP-containing suspensions is replotted as viscosity vs. shear stress in **Figure 6d** to confirm the presence of DST (slope of 1)[2] and identify τ_{min} and τ_{max}. The dependence of τ_{min} and τ_{max} on ϕ_{PVP} is presented in **Figure 8**. Interestingly, here increasing ϕ_{PVP} causes τ_{min} to increase (**Figure 8a**). This trend is opposite to that observed for the PVP-free suspensions in **Figure 4a**, in which increasing $\phi_{alumina}$ caused a decrease in τ_{min}. Non-adsorbing PVP is likely acting as a lubricant between particles,[55,56] decreasing the contribution of friction to stress which then increases the stress required for thickening. PVP addition also slightly increases τ_{max} (**Figure 8b**), following the same trend observed for alumina addition in **Figure 4b**, though τ_{max} levels off for $\phi_{PVP} = 0.03$-0.05. PVP may also be contributing to the frictional interaction networks during shear thickening, allowing suspensions with higher ϕ_{PVP} to endure higher stresses prior to failure. The rate of increase in both τ_{min} and τ_{max} in **Figure 8** is higher for $\phi_{PVP} = 0$-0.01 than for $\phi_{PVP} = 0.03$-0.05, suggesting that perhaps the polymer conformation (dilute vs. semi-dilute non-entangled) may affect the stress scaling of shear thickening.

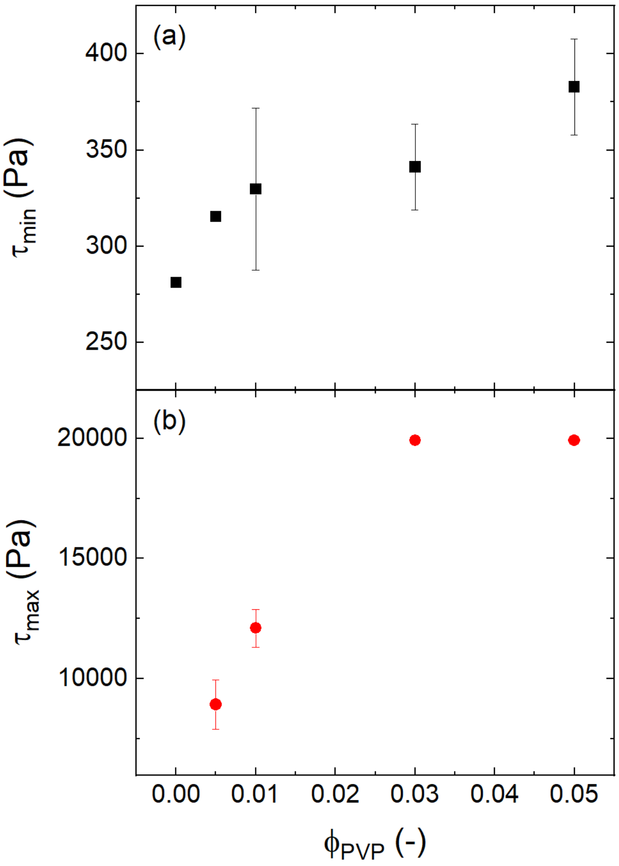

Figure 8. Average stress at (a) onset of thickening (τ_{min}) and (b) end of thickening (τ_{max}) for $\phi_{alumina} = 0.550$ suspensions at varying ϕ_{PVP}.

Finally, by directly comparing suspensions with and without PVP as shown in **Figure 9**, we demonstrate the benefits of increasing suspension viscosity and yield stress by non-adsorbing polymer addition as compared to the case of increasing the particle volume fraction. These sets of suspensions were selected for comparison because each pair exhibits similar rheology (viscosity magnitude and degree of shear thinning) prior to shear thickening. **Figure 9a** shows the flow curves for $\phi_{alumina} = 0.565$, $\phi_{PVP} = 0$ and $\phi_{alumina} = 0.550$, $\phi_{PVP} = 0.005$ plotted as viscosity vs. shear rate. It is observed that onset of shear thickening occurs at a higher shear rate for the PVP-containing suspension. This corresponds to an increase in τ_{min} for the PVP-containing suspension as visualized in **Figure 9b**. Similar trends are evident when comparing $\phi_{alumina} = 0.575$, $\phi_{PVP} = 0$ to $\phi_{alumina} = 0.550$, $\phi_{PVP} = 0.010$ in **Figures 9c-d**, where inclusion of PVP increases the onset shear rate of shear thickening and τ_{min} to an even further extent compared to its PVP-free counterpart than in **Figures 9a-b**. The τ_{max} values are lower for the PVP-containing suspensions in **Figures 9b** and **9d** as compared to the alumina-only suspensions, which can be attributed to the lower $\phi_{alumina}$ in the suspensions containing PVP. Increasing the onset shear rate and τ_{min} allows lower viscosity values and higher shear rates to be reached prior to shear thickening, extending the processing window for applications such as DIW. While a decrease in the viscosity and increases in the onset shear rate and τ_{min} could also be achieved by reducing $\phi_{alumina}$, doing so would occur at the expense of reducing τ_y, which would impede the formation of self-supporting layers and cause the printed parts to slump.[20,54]

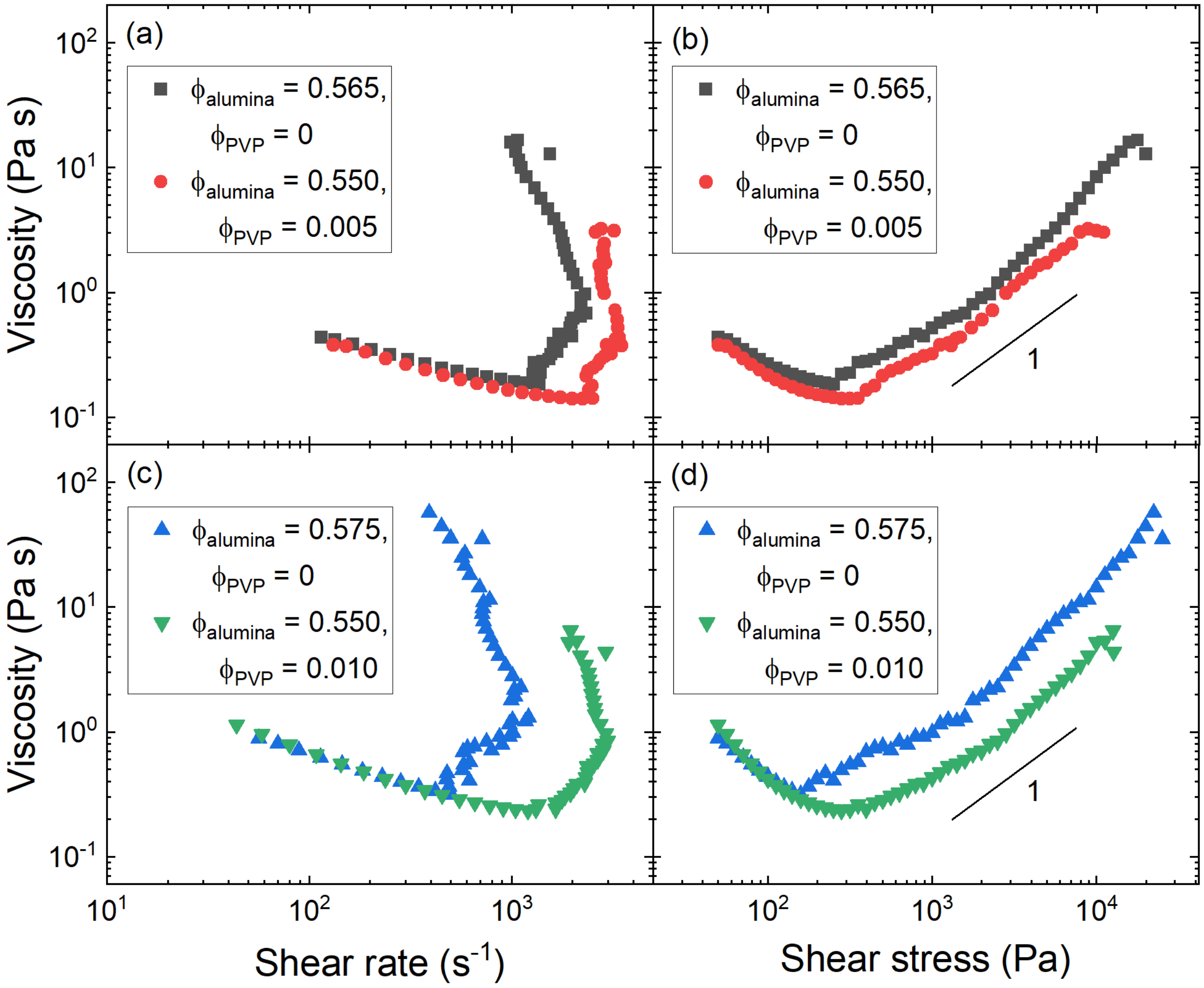

Figure 9. (a-b) Direct rheological comparison of $\phi_{alumina}$ = 0.565, ϕ_{PVP} = 0 to $\phi_{alumina}$ = 0.550, ϕ_{PVP} = 0.005 plotted as viscosity vs. shear rate (a) and viscosity vs. stress (b). (c-d) Direct rheological comparison of $\phi_{alumina}$ = 0.575, ϕ_{PVP} = 0 to $\phi_{alumina}$ = 0.550, ϕ_{PVP} = 0.010 plotted as viscosity vs. shear rate (c) and viscosity vs. stress (d).

CONCLUSIONS

We examined the effects of non-adsorbing PVP addition on the rheology of concentrated alumina suspensions. Increasing ϕ_{alumina} from 0.550 to 0.575 increased the viscosity and yield stress in the shear thinning regime. Shear thickening was observed in all cases above a composition-dependent value of $\tau_{\min}$, with DST observed for suspensions with $\phi_{\text{alumina}} \geq 0.560$ which were shown to be within a few percent of ϕj. Increasing ϕ_{alumina} decreased $\tau_{\min}$ and increased $\tau_{\max}$. Subsequently, we estimated that adding $\phi_{\text{PVP}} = 0.005\text{-}0.050$ to suspensions with constant $\phi_{\text{alumina}} = 0.550$ corresponded to dilute and semi-dilute non-entangled conformations of PVP. DST was exhibited at all PVP loadings and increasing ϕ_{PVP} increased the viscosity and yield stress in the shear thinning regime. Notably, increasing ϕ_{PVP} increased $\tau_{\min}$, presenting a trend opposite to that for increasing ϕ_{alumina}. We hypothesize that the presence of non-adsorbed PVP chains lubricate inter-particle contacts, reducing the frictional contribution to the overall stress and increasing the stress necessary to overcome repulsive forces between particles and induce thickening. Increasing ϕ_{PVP} also increased $\tau_{\max}$, suggesting that increasing solids through either polymer or particle addition imparts the ability to withstand higher stresses during shear thickening. Finally, we presented how the increased $\tau_{\min}$ caused by PVP addition could be advantageous during extrusion of multi-layered parts, permitting lower viscosity values and higher shear rates to be accessed prior to shear thickening (as compared to suspensions of higher ϕ_{alumina}) while sustaining similar values of τ_y necessary to maintain structural integrity.

Continued experimental work will explore the effects of varying non-adsorbing polymer MW on the rheology of concentrated particle suspensions. Scaling the polymer concentration to the overlap concentration (c*)[33] across a range of MWs may further elucidate how polymers influence the stress scaling of shear thickening, as we observed here that the rates of increase in

τ_{min} and τ_{max} diverged above c* (**Figure 8**). Incorporation of non-adsorbing polymers into computation models of particle suspensions will be necessary to confirm the mechanism(s) by which polymer addition affects inter-particle friction. Lastly, investigations into how variations in particle size, shape, and roughness affect interactions between particles and polymers of varying chemistry, length, architecture, and chain flexibility could yield rich insights into shear thickening suspension rheology and lead to the design of novel particle ink formulations for 3D printing.

AUTHOR CONTRIBUTIONS

R.D.C.: methodology, investigation, formal analysis, visualization, writing – original draft, and writing – review and editing. Y-J.C.: investigation. P.P.: investigation. J.P.Y.: conceptualization, resources, and writing – review and editing. A.M.A.: supervision and writing – review and editing. K.A.E.: conceptualization, supervision, and writing – review and editing.

ELECTRONIC SUPPLEMENTARY INFORMATION

Generalized Krieger-Dougherty model fitting of minimum and maximum relative viscosities and polymer solutions used to estimate concentration ranges for PVP conformations.

CONFLICTS OF INTEREST

There are no conflicts of interest to declare.

ACKNOWLEDGEMENTS

R.D.C. gratefully acknowledges support from the Lillian Gilbreth Postdoctoral Fellowship at Purdue Engineering. A.M.A acknowledges financial support from the National Science Foundation (NSF) through Grant No. CBET-2141404.

REFERENCES

1 N. J. Wagner and J. F. Brady, *Phys Today*, 2009, **62**, 27–32.

2 E. Brown and H. M. Jaeger, *Reports on Progress in Physics*, 2014, **77**, 046602.

3 J. Bender and N. J. Wagner, *J Rheol (N Y N Y)*, 1996, **40**, 899–916.

4 T. A. Prabhu and A. Singh, *J Rheol (N Y N Y)*, 2022, **66**, 731–747.

5 S. Dhar, S. Chattopadhyay and S. Majumdar, *Journal of Physics Condensed Matter*, 2020, **32**, 124002.

6 E. Brown and H. M. Jaeger, *J Rheol (N Y N Y)*, 2012, **56**, 875–923.

7 R. Seto, R. Mari, J. F. Morris and M. M. Denn, *Phys Rev Lett*, 2013, **111**, 218301.

8 E. Brown and H. M. Jaeger, *Phys Rev Lett*, 2009, **103**, 086001.

9 I. R. Peters, S. Majumdar and H. M. Jaeger, *Nature*, 2016, **532**, 214–217.

10 S. Pradeep, M. Nabizadeh, A. R. Jacob, S. Jamali and L. C. Hsiao, *Phys Rev Lett*, 2021, **127**, 158002.

11 R. v. More and A. M. Ardekani, *J Rheol (N Y N Y)*, 2020, **64**, 67–80.

12 C. P. Hsu, J. Mandal, S. N. Ramakrishna, N. D. Spencer and L. Isa, *Nat Commun*, 2021, **12**, 1477.

13 R. v More and A. M. Ardekani, *Phys Rev E*, 2021, **103**, 062610.

14 N. M. James, C.-P. Hsu, N. D. Spencer, H. M. Jaeger and L. Isa, *J. Phys. Chem. Lett*, 2019, **10**, 1663–1668.

15 R. Mari, R. Seto, J. F. Morris and M. M. Denn, *Proc Natl Acad Sci U S A*, 2015, **112**, 15326–15330.

16 S. Jamali and J. F. Brady, *Phys Rev Lett*, 2019, **123**, 138002.

17 M. A. S. R. Saadi, A. Maguire, N. T. Pottackal, M. S. H. Thakur, M. M. Ikram, A. J. Hart, P. M. Ajayan and M. M. Rahman, *Advanced Materials*, 2022, **34**, 2108855.

18 A. Shahzad and I. Lazoglu, *Compos B Eng*, 2021, **225**, 109249.

19 E. Feilden, E. G. T. Blanca, F. Giuliani, E. Saiz and L. Vandeperre, *J Eur Ceram Soc*, 2016, **36**, 2525–2533.

20 L. Rueschhoff, W. Costakis, M. Michie, J. Youngblood and R. Trice, *Int J Appl Ceram Technol*, 2016, **13**, 821–830.

21 Y. Lakhdar, C. Tuck, A. Terry, C. Spadaccini and R. Goodridge, *J Eur Ceram Soc*, 2021, **41**, 76–92.

22 H. A. Loh, A. R. Graves, C. D. Stinespring and K. A. Sierros, *ACS Appl Nano Mater*, 2019, **2**, 4104–4112.

23 M. Acosta, V. L. Wiesner, C. J. Martinez, R. W. Trice and J. P. Youngblood, *Journal of the American Ceramic Society*, 2013, **96**, 1372–1382.

24 A. Jain and E. S. G. Shaqfeh, *J Rheol (N Y N Y)*, 2021, **65**, 1269–1295.

25 E. S. G. Shaqfeh, *AIChE Journal*, 2019, **65**, e16575.

26 M. Yang and E. S. G. Shaqfeh, *J Rheol (N Y N Y)*, 2018, **62**, 1379–1396.

27 R. Scirocco, J. Vermant and J. Mewis, *J Rheol (N Y N Y)*, 2005, **49**, 551–567.

28 T. A. Prabhu and A. Singh, *Rheol Acta*, 2021, **60**, 107–118.

29 S. S. Shenoy and N. J. Wagner, *Rheol Acta*, 2005, **44**, 360–371.

30 L.-N. Krishnamurthy, N. J. Wagner and J. Mewis, *J Rheol (N Y N Y)*, 2005, **49**, 1347–1360.

31 Y.-F. Lee, Y. Luo, T. Bai, S. C. Brown and N. J. Wagner, *Soft Matter*, 2022, **18**, 4325–4337.

32 G. Bossis, P. Boustingorry, Y. Grasselli, A. Meunier, R. Morini, A. Zubarev and O. Volkova, *Rheol Acta*, 2017, **56**, 415–430.

33 N. Park, V. Rathee, D. L. Blair and J. C. Conrad, *Phys Rev Lett*, 2019, **122**, 228003.

34 E. Ordoñez, J. M. Gallego and H. A. Colorado, *Appl Clay Sci*, , DOI:10.1016/J.CLAY.2019.105285.

35 J. Liao, H. Chen, H. Luo, X. Wang, K. Zhou and D. Zhang, *J. Mater. Chem. C*, 2017, **5**, 5867.

36 E. Peng, X. Wei, U. Garbe, D. Yu, B. Edouard, A. Liu and J. Ding, *J Mater Sci*, 2018, **53**, 247–273.

37 A. U. Khan, B. J. Briscoe and P. F. Luckham, *Colloids Surf A Physicochem Eng Asp*, 2000, **161**, 243–257.

38 R. G. Horn, *Journal of the American Ceramic Society*, 1990, **73**, 1117–1135.

39 T. Kawasaki and L. Berthier, *Phys Rev E*, 2018, **98**, 012609.

40 M. Gameiro, A. Singh, L. Kondic, K. Mischaikow and J. F. Morris, *Phys Rev Fluids*, 2020, **5**, 34307.

41 V. Rathee, J. Miller, D. L. Blair and J. S. Urbach, *Proceedings of the National Academy of Sciences*, 2022, **119**, 203795119.

42 G. Ovarlez, A. Vu Nguyen Le, W. J. Smit, A. Fall, R. Mari, G. Chatté and A. Colin, *Sci Adv*, 2020, **6**, eaay5589.

43 T. Divoux, C. Barentin and S. Manneville, *Soft Matter*, 2011, **7**, 8409–8418.

44 S. Mueller, E. W. Llewellin and H. M. Mader, *Proceedings of the Royal Society A: Mathematical, Physical and Engineering Sciences*, 2010, **466**, 1201–1228.

45 N. M. James, H. Xue, M. Goyal and H. M. Jaeger, *Soft Matter*, 2019, **15**, 3649–3654.

46 J. E. Funk and D. R. Dinger, *American Ceramic Society Bulletin*, 1988, **67**, 890–894.

47 H. U. Kayacı and S. Çınar, *Ceram Int*, 2020, **46**, 20357–20368.

48 C. Ness and J. Sun, *Soft Matter*, 2016, **12**, 914–924.

49 E. Brown, H. Zhang, N. A. Forman, B. W. Maynor, D. E. Betts, J. M. Desimone and H. M. Jaeger, *Phys Rev E*, 2011, **84**, 031408.

50 M. Rubinstein and R. H. Colby, *Polymer Physics*, Oxford University Press, 2003.

51 A. el Aferni, M. Guettari, M. Kamli, T. Tajouri and A. Ponton, *J Mol Struct*, 2020, **1199**, 127052.

52 R. Wulfert, U. Seifert and T. Speck, *Soft Matter*, 2017, **13**, 9093–9102.

53 S. S. L. Chan, R. M. Pennings, L. Edwards and G. v. Franks, *Addit Manuf*, 2020, **35**, 101335.

54 H. Lombois-Burger, P. Colombet, J. L. Halary and H. van Damme, *Cem Concr Res*, 2008, **38**, 1306–1314.

55 H. Lombois-Burger, P. Colombet, J. L. Halary and H. van Damme, *Cem Concr Res*, 2006, **36**, 2086–2097.